Laser Induced Damage in Optical Materials; 1982 NBS Special Pub. 669, pp. 387-405

Temporal Dependence of Laser-Induced Breakdown in NaCl and SiO_2

M. J. Soileau, William E. Williams, Eric W. Van Stryland,
Thomas F. Boggess, and Arthur L. Smirl

Department of Physics
Center for Applied Quantum Electronics
North Texas State University
P. O. Box 5368
Denton, Texas 76203

The laser-induced damage (LID) thresholds of fused silica and single crystal NaCl were studied at wavelengths of 0.5 and 1 μm for pulses as short as 4 psec for a variety of focal spot sizes. The problem of sample-to-sample variation was minimized by performing parametric studies on a single sample at a time. Beam distortion measurements and polarization dependence studies of the LID thresholds demonstrate that the contribution of self-focusing to the LID measurements in this work was negligible. The damage threshold field, E_B, was found to increase as the pulsewidth was decreased in both materials at both wavelengths. The strongest pulsewidth dependence observed was approximately an inverse square root proportionality observed in NaCl at 1 μm for pulses shorter than 10 psec. For conditions of equal pulsewidth and the same focal spot size, E_B was less at 0.5 μm than at 1 μm for both materials.

Key Words: Laser Damage, Picosecond Pulses, Fused Silica, NaCl, Avalanche Breakdown, 1.06 μm, 0.53 μm, 1.05 μm.

1. Introduction

The problem of bulk laser-induced damage (LID) in nominally transparent materials has been the subject of extensive investigation [1]. However, after more than 15 years of study, bulk laser-induced damage is still not well understood. A major obstacle to developing models for such damage in highly transparent materials is the lack of a consistent data base for the dependence of LID on such basic parameters as laser wavelength and pulsewidth. The problems of sample to sample variations and the complex interdependence of the damage thresholds on laser frequency, pulsewidth, and focal conditions [2] make the interpretation of isolated data points difficult.

We have tried to minimize these problems by studying LID as a function of wavelength and pulsewidth for a variety of focal conditions on a given sample. In Ref. 2 the LID-thresholds of a sample of fused SiO_2 and a single cyrstal NaCl sample were studied at 1.06 μm as a function of pulsewidth for pulses ranging from 40 psec to 31 nsec using a variety of focal conditions. In that work we found that the laser-induced breakdown threshold field, E_B, (i.e., the r.m.s. field corresponding to the LID threshold peak-on-axis irradiance) was only weakly dependent on the laser pulsewidth. We found that, for the range of parameters used, we could fit all the data in Ref. 2 to the following empirical relationship

$$E_B = A/[t_p^{1/4}\ \omega_o^4] + B \qquad (1)$$

where A and B are constants for a given sample, t_p is the laser pulsewidth and ω_0 is the laser focal spot radius. In the present work, we find that this relationship breaks down for pulses shorter than 10 psec.

Here we extend the pulsewidth dependence studies at a wavelength of 1 μm to pulses as short as 4 psec, and we study the LID characteristics of fused SiO_2 and single crystal NaCl at 0.53 μm for pulsewidths in the 20 to 200 psec range. We find that the empirical relationship given by eq. 1 no longer holds for laser pulses shorter than 10 psec. For the shortest pulses (4 - 10 psec at 1.05 μm), E_B varied as approximately the inverse fourth root of the pulsewidth in SiO_2 and as approximately the inverse square root in NaCl for all the focal conditions studied.

For conditions of equal pulsewidth and the same focal spot size, E_B was less at 0.53 μm than at 1.06 μm for both materials for pulses in the 40 to 200 psec range. This result is contrary to the predictions of a simple avalanche breakdown model. Also, the observed dependence, while in the right direction, is much too weak for a strictly multiphoton process. A multiphoton initiated avalanche breakdown process [2] could possibly account for the observed wavelength dependence.

In addition, by carefully studying the polarization dependence of LID and by measuring the distortion of the transmitted beams, we show that the contribution of self-focusing to LID in our experiments is much less than has been assumed by other workers. In fact, for certain focal conditions we demonstrate that the effects of self-focusing are negligible.

2. Experiment

The lasers used in this study were a mode-locked Nd:YAG oscillator-amplifier system and a mode-locked Nd:Glass oscillator system which have been described elsewhere [2,3]. The YAG laser was operated at 1.06 μm and the glass at 1.05 μm. In each case a single pulse of measured Gaussian spatial and temporal profile was switched out of the mode-locked train and amplified. The pulsewidth of the Nd:YAG laser was varied from 40-200 psec by selecting various etalons as the output coupler of the oscillator. The glass laser pulsewidth varied from 4 to 10 psec. The pulsewidth and energy of each pulse were monitored. The width of each pulse was determined by monitoring the ratio of the energy in the second harmonic produced in a nonlinear crystal to the square of the energy in the fundamental. A more detailed description of energy and pulsewidth measurement are given in Ref. 2.

A temperature tuned CD*A crystal was used with the Nd:YAG laser to produce pulses at 0.53 μm. Care was taken to filter any residual 1.06 μm radiation from the 0.53 μm beam. The energy in the fundamental pulses at 1.06 μm was kept below a value which would produce saturation effects in the spatial profile of the second harmonic. Two-dimensional scans of the 0.53 μm beam with an optical multichannel analyzer (OMA) verified the absence of saturation effects and the Gaussian spatial profile of the 0.53 μm beam. Such vidicon scans of the spatial beam profile showed that the shot-to-shot variation in the beam width was less than our detection resolution limit of approximately 1%. Light-by-light scattering measurements in a $LiIO_3$ crystal [4] indicated that the 0.53 μm pulses had a Gaussian temporal shape. The results of these measurements confirmed that the 0.53 μm pulsewidth scaled as the 1.06 μm pulsewidth divided by $\sqrt{2}$. This scale factor was used to compute the 0.53 μm pulsewidths from the measured 1.06 μm pulsewidths.

The laser beam was focused into the bulk of the sample using single element, "best form", lenses designed for minimum spherical aberrations. Three lenses of focal lengths 37 mm, 75 mm, and 150 mm were used at various distances from the beam waist to produce the focal spot radii for these experiments. The lowest f-number condition used in these experiments was f/10.3. In each case, the

beam diameter was kept below maximum values necessary to ensure diffraction limited performance. Aberrations caused by focusing through the planar surfaces of the samples were calculated to cause an error in the field of less than 0.1% for the worst case. The output energy of the CD*A crystal was monitored continually using a sensitive photodiode peak-and-hold detector, absolutely calibrated with respect to a pyroelectric energy detector. Transmission through the sample was monitored by another peak-and-hold detectors.

In some cases, the transmission detector was replaced by a vidicon tube used in conjunction with an optical multichannel analyzer to scan the transmitted beam profile. Such scans were made at the damage threshold irradiance and for irradiance levels ten times below the damage threshold. In this way, a total time integrated beam distortion at the beam waist of the order of $\lambda/5$ could be detected.

The short pulsewidth data (4-9 psec) were taken on the same samples using a microprocessor-controlled Nd:Glass oscillator system operating at a laser wavelength of 1.05 μm [3]. This system produced single pulses of measured Gaussian spatial profile. Shot-to-shot energy fluctuations were determined to be ~20%. The same focusing lenses were used as with the 0.53 μm measurements. Beam scans as a function of distance from the laser were employed (as was also done using the 1.06 μm laser) to determine the beam divergence (0.4 mrad.) and the position and size of the output beam waist. This information and the lens focal length were then used to calculated the beam waist at the lens focus. Energy on target was varied using a calibrated Glan polarizer. The procedures for measuring and continuously monitoring both pulsewidth and energy are identical to those described previously with the Nd:YAG laser system [2].

The breakdown threshold for a given pulsewidth was taken to be that irradiance which produced damage 50% of the time. Each site was irradiated only once. Damage was defined as the appearance of a visible flash in the bulk of the sample or by the observation of forward scattered light from a coaxial HeNe laser as viewed through a ten-power long-working distance microscope. The microscope also was used to verify that damage had occured at the beam focus and was not due to inclusions. For 0.53 μm damage, the appearance of 0.53 μm scattered radiation and HeNe scattered light occurred simultaneously for both SiO_2 and NaCl. In the cases of the 4-9 psec 1 μm data, for both SiO_2 and NaCl, there was a small range of incident energies where damage had occured as determined from scattered HeNe radiation, but no flash was observed. N-on-1 experiments (multiple shot irradiation at the same sample site) conducted at both wavelengths, indicate no change in the breakdown threshold when compared to the 1-on-1 experiments (only one irradiation per sample site).

3. Self-Focusing Considerations

In order to produce laser-induced damage in the bulk of a highly transparent material one must tightly focus the light into the material. Since the beam propagates through the material, one must consider the effects of self-focusing on the results of bulk damage measurements, particularly when the power required to induce damage is of the order of the predicted critical power for self-focusing. Marburger [5] has derived an approximate solution to the nonlinear wave equation for a focused Gaussian beam in a nonlinear medium. This solution (called the constant shape approximation) assumes that, in the presence of self-focusing, the focused beam waist is given by

$$a = (1 - P/P_1)^{1/2} a_o \qquad (2)$$

where P_1 is the critical power for self-focusing

a_o is the focal radius in the absence of self-focusing, and

P is the input power.

Some workers have assumed that the damage threshold irradiance for highly transparent materials (such as those used in this study) is an intrinsic property [6] of the material and that any apparent dependence of the breakdown irradiance on a_o is due to self-focusing [7,8,9] The breakdown power then was measured for various values of a_o and the results fit to the equation

$$1/P_B = 2/I_B \pi a_o^2 + 1/P_1 \tag{3}$$

where P_B is the power required for breakdown and

I_B is the intrinsic damage threshold.

A number of authors have used this technique to extract values for I_B and P_1 for nanosecond [7,8] and picosecond pulses [10,11] In some cases P_1 was calculated [11] in accordance with the relation [5]

$$P_1 = c\lambda^2/32\pi n_2 \tag{4}$$

where λ is the wavelength, and n_2 is the nonlinear refractive index. A new focal radius was calculated using eq. (1). The n_2 values used in these calculations were taken from nanosecond measurements.

There are serious problems associated with using the above mentioned procedure. Subsequent work has shown that I_B is not an intrinsic property of a transparent material as evidenced by large sample to sample variations observed in a given material [2,12]. A second problem is that other self-action effects such as a saturation of the self-focusing or free carrier defocusing may become important at the extremely high irradiance levels required for damage. The presence of these "free" electrons creates a negative change in the index of refraction which can limit the self-focus collapse, [5,13,15] defeat self-focusing entirely, [15] and in some cases lead to self-defocusing of the beam. [16,17] Therefore, before any analysis of damage data can begin, one needs to devise tests which will verify the presence, or absence of self-focusing effects.

One such test arises directly from self-focusing theory which predicts that the critical power for self-focusing is lower for linearly polarized light compared to that for circularly polarized light [18-21]. Experimental measurements in liquids, such as CS_2, conducted by ourselves [22] and others [20,23] have confirmed that this is indeed the case. In solids, Feldman et al. [19] measured ratios of circular polarization thresholds to linear polarization thresholds on the order of 1.1 to 1.3 for fused quartz. These measurements were conducted using nanosecond pulses at 1.06 μm where both electrostrictive and electronic contributions to n_2 are believed to be important. For picosecond pulses the dominant contribution to n_2 is believed to be electronic self-focusing, which is polarization dependent. Thus, if self-focusing effects are important in our measurements, then the breakdown thresholds should be different for different polarization configurations.

In figure 1 we present the results of polarization dependent studies for a sample of fused quartz at a laser wavelength of 0.53 μm and 1.06 μm. The breakdown thresholds are given in terms of the r.m.s. electric field, in MV/cm, corresponding to the peak-on-axis irradiance producing damage. In both cases we used the shortest pulses available to us, which corresponded to the highest input

power for the given focal spot radius of 5 μm (HW $1/e^2$ M). As can be seen the breakdown field for linear polarization equals that for circular polarization. In both materials no polarization dependence was observed for pulses between 4-9 psec (FWHM) at 1.05 μm even for the largest spot size used in this study. Similar results were obtained in measurements on a NaCl sample at a 0.53 μm laser wavelength for 30 psec pulses. Thus, for the focal conditions used, we observed no polarization dependence of the breakdown thresholds for either fused quartz or NaCl.

Another, independent test for the presence of self-focusing is to examine the beam spatial profile after transmission through the sample for irradiance levels far below and near the damage threshold. In figure 2 we show two vidicon traces taken in the far field through the center of the 0.53 μm beam after transmission through the fused quartz sample. The focal spot radius (HW $1/e^2$ M) at the beam waist for this configuration, in the absence of self-focusing, in approximately 7 μm. The solid trace was taken near the damage threshold. The dashed trace was taken at an irradiance level approximately 10 times below the damage threshold. Filters were placed in front of the vidicon to adjust the irradiance at the vidicon surface to the same value in both traces in order to minimize any problems in detector nonlinearity. Inspection of figure 2 shows no detectable beam distortion for input powers approximately equal to the damage threshold power. Scans conducted for a focal spot size of 3.4 μm at the 0.53 μm laser wavelength also show no distortions.

The authors are aware that the technique just described monitors the time-integrated beam spatial profile; however, this technique is sensitive to a $\lambda/5$ distortion in the total time integrated profile and has proven to be a sensitive technique for monitoring the onset of self-defocusing in solids [16]. These measurements, when taken together with the polarization experiments described above, indicate that self-focusing effects were not important for the geometries used in these experiments. However, the reader should be aware that in other experimental geometries (i.e., less tightly focused beams) self-focusing effects can be important. In fact, preliminary measurements in SiO_2 at 0.53 μm indicate that for a 14 μm focal spot radius the far field beam radii for irradiance at the damage threshold differs from that at low irradiance levels by approximately 28% (indicating that self-focusing has taken place). For that same focal geometry the ratio of the LIB threshold for circularly polarized light to that for linearly polarized light is approximately 1.4. These self-focusing studies are not yet complete and will be reported in detail at a later date. We emphasize that no data are included in this paper for which either the polarization test or the beam distortion test indicate the presence of self-focusing.

4. Experimental Results and Discussions

Tables I-VIII summarize the results of measurements of the laser-induced breakdown thresholds for two different samples of single crystal NaCl and fused silica [24]. The NaCl sample labeled 78-NC-6 is the same sample used in previous picosecond damage studies [2] and in studies at longer pulsewidths and wavelengths [15,25]. Both SiO_2 samples have been used in nanosecond studies at 1.06 μm [26] and the sample labeled 79-FQ-125-1 was used in previous picosecond studies [2]. The uncertainties listed in the tables of data are the relative errors obtained by the method of Porteus et al. [27]. The absolute errors, which include the relative errors and absolute errors in energy, pulsewidth and focal spot radius, are estimated to be ±20% in the breakdown electric fields.

Tables I-IV summarize the results of our measurements at 0.53 μm for laser pulsewidths in the 25 to 200 psec (FWHM) range. These results will be compared here with the results of our earlier studies at 1.06 μm for these same materials over a similar range of pulsewidths. Tables V-VIII contain the results of measurements on these same samples at 1.05 μm for pulses in the 4 - 10 psec

range. In addition, Tables VI and VIII contain LID thresholds at 1 μm in the pulsewidth range of 40 to 200 psec for a 7.2 μm focal spot radius. These thresholds are taken from our previous work (Ref. 2) and were interpolated from measurements made at focal spot size of 6.1 and 10.3 μm.

In the paragraphs that follow, we examine the pulsewidth dependence of the threshold breakdown field, E_B, for a given sample at a given wavelength and focal spot radius. We then examine the wavelength dependence of E_B for a given pulsewidth and spot size.

The dependence of E_B on pulsewidth (t_p) is more clearly seen by plotting E_B versus the inverse pulsewidth on a log-log plot. Figures 3 and 4 are such plots for a NaCl sample (82-NC-1) and a SiO_2 sample (79-FQ-7940-1) at 1.05 μm. Note that for a given spot size and for pulses shorter than 10 psec the data for each sample can be fit with a straight line. Over this limited pulsewidth range

$$E_B \propto t_p^{-x} \tag{5}$$

where $x \approx 0.3$ for the SiO_2 sample and $x \approx 0.5$ for the NaCl sample. The displacement of each set of data points corresponding to different focal spot sizes indicates a relatively strong spot size dependence in these samples at this wavelength.

Figures 5 and 6 are similar plots for the same two samples (79-FQ-7940-1 and 82-NC-1) at 0.53 μm for pulsewidths in the 25-200 psec range. Again one can fit the data with a linear dependence. However, in this case $x < 0.1$ for the SiO_2 sample and $x \approx 0.3$ for the NaCl sample. Similar trends are seen in the data for the other SiO_2 and NaCl samples given in tables II, IV, VI, and VIII.

At 0.53 μm and 1.06 μm the pulsewidth dependence of E_B observed for both materials is in good agreement with the predictions of various avalanche breakdown models [28,29,30]. For example the model proposed by Sparks et al. [28] predicts very little pulsewidth dependence for relatively long pulses (nsec) and a dependence of E_B on pulsewidth which approaches an inverse square root dependence for relatively short pulses, i.e., ten's of picoseconds. The inverse square root of pulsewidth dependence implies that the breakdown fluence is constant (as can be seen in tables VII and VIII for the NaCl samples). We find that for NaCl in the long pulsewidth limit ($t_p > 1$ nsec) the breakdown field is nearly constant, whereas in the short pulsewidth limit ($t_p < 10$ psec) the breakdown fluence is nearly constant. The trend in the t_p dependence of E_B for SiO_2 is similar to that seen in NaCl, however, the strongest dependence of E_B on t_p observed was $E_B \propto t_p^{-0.3}$ for pulses shorter than 10 psec at 1.05 μm. It is important to note that the strongest pulsewidth dependence of E_B observed in these measurements was the approximate inverse square root of pulsewidth dependence observed for NaCl for $t_p < 10$ psec at 1.05 μm. In an avalanche breakdown model this dependence implies an ionization rate (β) which is proportional to the input irradiance. Then the buildup of carriers is given by [28]

$$N = N_o e^{\beta t} = N_o e^{AE^2 t} \tag{6}$$

where N is the carrier density

N_o is the initial carrier density or carrier density produced by multiphoton ionization.

A is constant.

It is commonly assumed that damage occurs when the carrier density reaches a critical value, N_c. Thus eq. 2 gives the following relationship for E_B

$$E_B = (1/\sqrt{\tau_p})\, \ell n\, [(N_c/N_o)/A]^{1/2} \qquad (7)$$

and the [] term is constant for a given sample and laser frequency. The breakdown fluence, ϵ_B, is proportional to E_B^2 times the laser pulsewidth. Therefore eq. 6 implies that ϵ_B is a constant for β proportional to E^2.

In the Sparks avalanche breakdown model the ionization rate β is proportional to E^2 in the high electric field limit. This limit corresponds to the situation in which the increase in energy of the electrons in the conduction band is simply proportional to the input irradiance and that all losses are negligible. This simply says that the ionization rate is limited by the rate at which the input light beam can supply energy to the conduction band electrons. For the low field limit, i.e. longer pulses, β is exponentially dependent on E and the resulting pulsewidth dependence is relatively weak. In figure 7, we have reproduced the theoretical curves derived by Sparks et al. [28] showing the predicted dependence of the breakdown electric field, E_B, on pulsewidth and have extended the pulsewidth scale to longer and shorter pulsewidths. These curves were obtained by numerical integration of the Fokker Planck diffusion equation with appropriate boundary conditions reflecting energy loss by electrons to phonons. The solid curve was obtained using a value for σ_{Cl}, the electron-chlorine ion scattering cross section, taken from atomic physics literature. The dotted curve labled "σ_{Cl} adjusted" was obtained using a value for this parameter adjusted so as to give a better fit to experimental LID data available at the time. This cross section appears in the equations used to calculate the electron-phonon relaxation frequencies. The experimental points shown were obtained in this work at 1.05 μm for the NaCl sample labeled 78-NC-6 (Table VIII) and in our previous picosecond study at 1.06 μm [2]. Note the excellent agreement between the Sparks avalanche model and the data obtained here and in Ref. 2 for the 5 μm spot size. Data obtained in the same sample for a larger spot size (7.2 μm) show a similar trend in the functional dependence of E_B on pulsewidth but the values of E_B are lower than those given by this model. The agreement between the absolute values predicted by theory and experiment for 5 μm spot size may be fortuitous since the Sparks model describes intrinsic avalanche breakdown, i.e., the starter electrons necessary to create the avalanche are assumed to be already present. Such a model predicts no spot size dependence of the breakdown field. The relatively strong spot size dependence observed in NaCl at 1.06 μm indicates that damage in this material is probably initiated by some extrensic process; for example, multiphoton ionization of material defects.

Other workers have used an approximate inverse pulsewidth dependence (i.e., x = 1 in eq. 3) to scale breakdown data for various materials [11]. This is a much stronger dependence than is observed in this work. Their strong pulsewidth dependence was determined by combining the 1.06 μm, 30 psec data in Ref. 9 and 1.06 μm, 15 psec data in Ref. 31. These two data points were taken with different focal spot sizes. That is, the 30 psec data point in Ref. 9 was taken with relatively small focal radii (4.7 to 5.9 μm $1/e^2$ radius) and was reduced with the assumption that self-focusing was dominating the observed damage. The 15 psec data point in Ref. 31 was taken with a relatively large focal radius (12.4 μm HW $1/e^2$ M) and thus higher input power. In the latter work the authors assumed that self-focusing was not present in their experiment. The relatively large pulsewidth

dependence deduced from these two isolated data points is probably due to differences in experimental conditions used in these two measurements and the different methods of data reduction.

We now examine the wavelength dependence of the breakdown thresholds for laser pulsewidths in the 25 - 200 psec range. In figure 8 we have plotted, in bar graph form, the breakdown electric fields for SiO_2 (sample 79-FQ-125-1) and NaCl (sample 78-NC-6) for 1.06 μm and 0.53 μm for various pulsewidths at a fixed focal spot radius (7.2 μm). The 1.06 μm LID thresholds at the 7.2 μm focal radius are taken from Ref. 2 and are interpolated from measurements at spot sizes of 6.1 and 10.3 μm. In two cases where the pulsewidths did not exactly overlap for the two wavelengths we interpolated the 0.53 μm data between two pulsewidths for which data was available. This procedure was made necessary by the fact that only a limited number of pulsewidths were available at each wavelength studied. The errors due to interpolation are estimated to be within the error bars shown in figure 8.

Note that for each pulsewidth range plotted in figure 8 the breakdown field is less at 0.53 μm than at 1.06 μm for both the SiO_2 and the NaCl sample. Avalanche breakdown theory predicts an increase in E_B with decreasing wavelength, which is clearly inconsistent with the results shown in figure 8. The observed decrease in breakdown field with wavelength, while in the right direction, is much too weak for a strictly multiphoton process. One could possibly account for these results by a multiphoton initiated avalanche breakdown model which has been previously suggested.

Smith et al. [11] observed an increase in the breakdown threshold with decreasing wavelength for picosecond pulses. However, the data presented in that work was scaled for the presumed effects of self-focusing using eq. (2) for 1.06 μm and eq. (1) for 0.53 μm over a range of pulsewidths and spot sizes in which we observe no such effects. In addition it is unclear whether the same samples were used in the wavelength comparison. Manenkov [12] observed an initial increase in the damage threshold for a sample of NaCl from 1.06 μm, to 0.69 μm, then a decrease in the damage threshold at 0.53 μm for pulses ranging from 15 to 8 nsec. The data presented in that work was not scaled for self-focusing.

5. Summary

Laser-induced breakdown was studied as a function of pulsewidth and wavelength for a variety of focal conditions in fused SiO_2 and single crystal NaCl. Beam quality measurements and polarization dependence studies indicated the absence of self-focusing effects in these experiments such that no self-focusing corrections need be used.

For the two materials studied the breakdown field (E_B) increases with decreasing pulsewidth. The observed pulsewidth dependence for a given spot size and wavelength is consistent with the pulsewidth dependence predicted by various electron avalanche breakdown models. However, the spot size dependence observed in this study is not predicted by any avalanche theory and is probably due to the extrinsic nature of the observed damage. The strongest pulsewidth dependence observed was in NaCl at 1.05 μm for pulses shorter than 10 psec. For these short pulses E_B increases as the inverse square root of the pulsewidth, indicating that the breakdown fluence is constant.

For conditions of equal pulsewidth and the same focal spot size, i.e., pulsewidths from 45 to 175 psec and a focal spot size of 7.2 μm, E_B is less at 0.53 μm than at 1.06 μm for both materials. Avalanche breakdown theories predict an increase in E_B for shorter wavelengths. The observed decrease in breakdown field with wavelength, while in the right direction, is much too weak for a strictly multiphoton process. A multiphoton-initiated avalanche breakdown process might account for these results. In such a process electrons are excited to the conduction band by multiphoton

excitation of impurities or defect states within the material bandgap (i.e., extrinsic effects). After a few electrons are present in the conduction band, avalanche ionization takes over and dominates the damage process. Thus, the frequency dependence observed may be partly due to the multiphoton initiation process and the pulsewidth dependence indicative of an avalanche ionization process.

The authors acknowledge the support of the Office of Naval Research, the National Science Foundation, The Robert A. Welch Foundation, and the North Texas State University Faculty Research Fund.

References

[1] A central depository of work in this area are the proceedings of the symposium on "Laser-Induced Damage in Optical Materials", National Bureau of Standards Special Publications, #341 (1970), #356 (1971), #372 (1972), #387 (1973), #414 (1974), #435 (1975), #462 (1976), #509 (1977), #541 (1978), #568 (1979), #620 (1980). These may be obtained from the Superintendent of Documents, U.S. Government Printing Office Washington, D.C. 20402. Papers in these proceedings contain further reference to materials in this field.

[2] E. W. Van Stryland, M. J. Soileau, Arthur L. Smirl, and William E. Williams, Phys. Rev. B 23, 2144 (1981).

[3] A. L. Smirl, T. F. Boggess, B. S. Wherrett, G. P. Perryman, and A. Miller, IEEE J. Quantum Electron. (to be published).

[4] E. W. Van Stryland, W. E. Williams, M. J. Soileau, and A. L. Smirl, to be published in the Proceedings of the 1981 Conference on Laser-Induced Damage in Optical Materials, Boulder, Colorado.

[5] J. Marburger, in Progress in Quantum Electronics edited by J. H. Sanders and S. Stenhold (Pergamon, Oxford, 1975), Vol. 4, Part 1, and references therein.

[6] Nicolass Bloembergen, IEEE J. Quantum. Electron. QE-10, 375 (1974).

[7] G. M. Zverev and V. A. Pashkov, Sov. Phys. JETP, Vol. 30, 616 (1970).

[8] D. W. Fradin, IEEE J. Quantum Electron. QE-9, 954 (1972).

[9] W. Lee Smith, J. H. Bechtel, and N. Bloembergen, Phys. Rev. B 12, 706 (1975).

[10] W. Lee Smith and J. H. Bechtel, Appl. Phys. Lett. 28, 606 (1976).

[11] W. L. Smith, J. H. Bechtel, and N. Bloembergen, Phys. Rev. B 15, 4039 (1977).

[12] A. A. Manenkov, Natl. Bur. Stand. (U.S.) Spec. Publ. 509, 455 (1977).

[13] R. W. Hellworth, Natl. Bur. Stand. (U.S.) Spec. Publ. 341, 67 (1970).

[14] E. Yablonovitch and N. Bloembergen, Phys. Rev. Lett. 29, 907 (1972).

[15] M. J. Soileau, Ph.D. Thesis, University of Southern California, 1979, unpublished.

[16] E. W. Van Stryland, A. L. Smirl, T. F. Boggess, and F. A. Hopf, in Picosecond Phenomena III (Springer-Verlag, New York, 1982), p. 368.

[17] P. Kelly, A. Schmid, and P. Braunlich, Phys. Rev. B 20, 815 (1979).

[18] Y. R. Shen, Phys. Rev. Lett. 20, 378 (1966).

[19] A. Feldman, D. Horowitz, and R. Waxler, Natl. Bur. Stand. Spec. Publ. 372, 92 (1972).

[20] C. C. Wang, Phys. Rev. 152, 149 (1966).

[21] R. W. Hellworth, Progress in Quantum Electronics, Vol. 5, pp. 1-68, Pergamon Press, N.Y., 1977.

[22] M. J. Soileau, W. E. Williams, E. W. Van Stryland, and S. F. Brown, Proceedings of the Conference on Laser Induced Damage to Optical Materials, 1981, to be published by Natl. Bur. Stand. Spec.

[23] D. H. Close, C. R. Giuliano, R. W. Hellworth, L. D. Hess, F. J. McClung, and W. G. Wagner, IEEE J. Quant. Electron. QE-2, 553 (1966).

[24] The fused silica samples were acquired from Mark Optics, 1510 East St. Gertrude Road, Santa Ana, CA 92705. The SiO_2 designated 78-FQ-125-1 was a General Electric #125, high purity water free sample and the sample designated 78-FQ-7940-1 was a Corning #7940 sample which contained substantial water, but is otherwise a high purity material. Both NaCl samples were single crystal "laser grade" material from the Harshaw Chemical Co., 6801 Cochran Road, Solon, Ohio 44139.

[25] M. J. Soileau, M. Bass, and P. H. Klein, NBS Special Publ. 568, p. 497 (1979).

[26] M. J. Soileau and M. Bass, IEEE Journal of Quantum Electronics QE-16, 814 (1980).

[27] J. O. Porteus, J. L. Jernigan, W. N. Faith, NBS Spec. Pub. 509, 507 (1977).

[28] M. Sparks, T. Holstein, R. Warren, D. L. Mills, A. A. Maradudin, L. J. Shan, E. Loh Jr., and F. King, NBS Spec. Publ. 568, 467 (1979).

[29] S. Brawer, Phys. Rev. B 20, 3422 (1979).

[30] A. S. Epifanov, IEEE Journal of Quantum Electron. QE-17, 2018 (1981).

[31] D. W. Fradin, N. Bloembergen, and J. P. Lettlier, Appl. Phys. Lett. 22, 635 (1973).

Table I. LID data for sample 79-FQ-7940-1 (SiO_2) at 0.53 μm. The error values listed are the relative uncertainties in the threshold for damage determined by the method used in Ref. 27. The absolute accuracy of this data and the data presented in the other tables is estimated to be ±20% in the breakdown field. In this table and those that follow W = focal spot radius (HW $1/e^2$ M) in microns, τ_0 = laser pulsewidth (FWHM) in psec, I_B = breakdown irradiance, E_B = breakdown field, P_B = breakdown power and ϵ_B = breakdown fluence.

W (μm)	τ_0 (psec)	I_B (TW/cm^2)	E_B (MV/cm)	P_B (MW)	ϵ_B (J/cm^2)
7.2	25 ± 4	1.32 ± 0.13	18.3 ± 0.9	1.07 ± 0.11	35.0 ± 3.5
	53 ± 5	0.78 ± 0.08	14.1 ± 0.7	0.64 ± 0.06	44.0 ± 4.4
	110 ±10	0.78 ± 0.08	14.1 ± 0.7	0.64 ± 0.06	91 ± 9
5.0	37 ± 5	1.40 ± 0.14	18.9 ± 0.9	0.55 ± 0.06	55 ± 6
	105 ±15	1.20 ± 0.12	17.5 ± 0.8	0.47 ± 0.05	134 ± 13
	140 ±15	1.14 ± 0.11	17.0 ± 0.8	0.45 ± 0.05	169 ± 17
	180 ±20	1.10 ± 0.11	16.7 ± 0.7	0.43 ± 0.04	210 ± 21
3.4	30 ± 5	1.68 ± 0.17	20.7 ± 1.0	0.31 ± 0.03	53 ± 5
	72 ±10	1.34 ± 0.13	18.5 ± 0.8	0.24 ± 0.02	102 ± 10
	105 ±15	1.07 ± 0.11	16.5 ± 0.8	0.19 ± 0.02	83 ± 8

Table II. LID data for sample 79-FQ-125-1 (SiO_2) at 0.53 μm. See Table I for explanation of symbols and error bars.

W (μm)	τ_0 (psec)	I_B (TW/cm^2)	E_B (MV/cm)	P_B (MW)	ϵ_B (J/cm^2)
7.2	25 ± 4	0.96 ± 0.10	15.7 ± 0.8	0.79 ± 0.08	25.5 ± 3.0
	105 ± 15	0.48 ± 0.05	11.0 ± 0.5	0.39 ± 0.04	53 ± 5
	150 ± 15	0.39 ± 0.06	9.9 ± 0.8	0.32 ± 0.04	62 ± 6
5.0	34 ± 4	1.02 ± 0.10	16.1 ± 0.8	0.40 ± 0.04	37 ± 4
	120 ± 15	0.86 ± 0.09	14.8 ± 0.7	0.34 ± 0.03	109 ± 11
	180 ± 20	0.80 ± 0.15	14.3 ± 1.0	0.32 ± 0.03	153 ± 25
3.4	32 ± 4	1.16 ± 0.15	17.2 ± 1.0	0.21 ± 0.02	39 ± 4
	120 ± 15	0.91 ± 0.09	15.2 ± 0.5	0.16 ± 0.02	115 ± 12
	180 ± 20	0.75 ± 0.12	13.8 ± 1.0	0.14 ± 0.01	143 ± 14

Table III. LID data for sample 82-NC-1 (NaCl) at 0.53 μm.

W (μm)	τ_p (psec)	I_B (GW/cm^2)	E_B (MV/cm)	P_B (KW)	ϵ_B (J/cm^2)
14.0	35 ± 4	57 ± 6	3.80 ± 0.25	174 ± 17	2.10 ± 0.20
	80 ± 8	35 ± 4	2.98 ± 0.15	107 ± 10	2.96 ± 0.30
	110 ± 15	32 ± 3	2.87 ± 0.15	100 ± 10	3.77 ± 0.38
7.2	41 ± 9	91 ± 9	4.80 ± 0.35	120 ± 12	3.95 ± 0.40
	82 ± 7	64 ± 6	4.03 ± 0.19	40 ± 4	5.50 ± 0.60
	120 ± 15	47 ± 5	3.45 ± 0.19	29 ± 3	6.00 ± 0.60
3.4	26 ± 4	139 ± 14	5.95 ± 0.48	26.0 ± 0.3	3.83 ± 0.38
	37 ± 3	115 ± 12	5.41 ± 0.33	21.0 ± 0.2	4.50 ± 0.50
	57 ± 3	95 ± 9	4.64 ± 0.30	15.0 ± 0.2	5.10 ± 0.50
	73 ± 4	71 ± 7	4.24 ± 0.52	12.8 ± 0.12	5.50 ± 0.60
	90 ± 10	64 ± 6	4.04 ± 0.18	12.0 ± 0.12	6.10 ± 0.60
	115 ± 15	35 ± 4	3.00 ± 0.31	6.4 ± 0.54	4.30 ± 0.40

Table IV. LID data for sample 78-NC-6 (NaCl) at 0.53 μm.

W (μm)	τ_p (psec)	I_B (GW/cm^2)	E_B (MV/cm)	P_B (KW)	ϵ_B (J/cm^2)
14.0	25 ± 5	120 ± 12	5.53 ± 0.33	370 ± 40	3.19 ± 0.32
	105 ± 15	48 ± 5	3.50 ± 0.20	148 ± 15	5.37 ± 0.54
	170 ± 20	34 ± 6	2.95 ± 0.30	105 ± 10	6.18 ± 0.62
7.2	30 ± 5	148 ± 15	5.14 ± 0.30	120 ± 12	4.72 ± 0.47
	105 ± 15	60 ± 5	3.55 ± 0.20	40 ± 4	5.53 ± 0.56
	150 ± 15	36 ± 4	3.03 ± 0.16	29 ± 3	5.74 ± 0.57
3.4	23 ± 4	184 ± 18	6.86 ± 0.31	33.0 ± 3.3	5.48 ± 0.55
	85 ± 5	82 ± 8	4.56 ± 0.23	15.0 ± 1.5	7.39 ± 0.74
	100 ± 10	66 ± 7	4.10 ± 0.21	12.0 ± 1.2	7.02 ± 0.70
	120 ± 10	55 ± 8	3.75 ± 0.30	10.0 ± 1.0	7.05 ± 0.71
	140 ± 10	44 ± 7	3.35 ± 0.30	8.0 ± 0.8	6.57 ± 0.66
	170 ± 20	34 ± 5	2.95 ± 0.21	6.0 ± 0.6	6.17 ± 0.62

Table V. LID data for sample 79-FQ-7940-1 (SiO_2) at 1.05 μm.

W (μm)	t_p (psec)	I_B (TW/cm^2)	E_B (MV/cm)	P_B (MW)	ε_B (J/cm^2)
14.0	7.9 ± 0.6	1.12 ± 0.11	16.8 ± 0.8	3.44 ± 0.34	9.4 ± 0.9
	6.3 ± 0.3	1.25 ± 0.13	17.7 ± 1.0	3.84 ± 0.38	8.4 ± 0.8
	5.2 ± 0.3	1.42 ± 0.14	18.9 ± 1.0	4.37 ± 0.44	6.9 ± 0.6
	3.6 ± 0.3	1.75 ± 0.18	21.0 ± 1.1	5.39 ± 0.54	6.7 ± 0.7
7.2	8.5 ± 0.5	2.27 ± 0.23	24.1 ± 1.1	1.85 ± 0.19	20.5 ± 2.0
	7.5 ± 0.5	2.20 ± 0.22	23.7 ± 1.1	1.79 ± 0.18	17.5 ± 1.8
	6.5 ± 0.5	2.60 ± 0.26	25.7 ± 1.3	2.12 ± 0.21	18.0 ± 1.8
	5.5 ± 0.5	2.75 ± 0.28	26.5 ± 1.2	2.24 ± 0.22	16.1 ± 1.6
	4.5 ± 0.5	3.14 ± 0.31	28.3 ± 1.3	2.56 ± 0.26	15.0 ± 1.5
	3.6 ± 0.4	3.65 ± 0.37	30.5 ± 1.5	2.97 ± 0.30	14.0 ± 1.4
5.0	8.5 ± 0.5	3.04 ± 0.30	27.8 ± 1.4	1.19 ± 0.12	27.6 ± 2.8
	7.5 ± 0.5	3.24 ± 0.32	28.7 ± 1.3	1.27 ± 0.13	25.9 ± 2.6
	6.5 ± 0.5	3.56 ± 0.37	30.1 ± 1.5	1.40 ± 0.14	24.6 ± 2.5
	5.5 ± 0.5	3.94 ± 0.39	31.7 ± 1.5	1.55 ± 0.16	23.1 ± 2.3
	3.6 ± 0.3	5.00 ± 0.60	35.7 ± 2.0	1.96 ± 0.20	19.2 ± 1.9

Table VI. LID data for sample 79-FQ-125-1 (SiO_2) at 1.05 μm. The data for 7.2 μm size and t_p = 47 to 175 psec is taken from Ref. 2 and is interpolated from measurements made at spot sizes of 6.1 and 10.3 μm and a laser wavelength of 1.06 μm.

W (μm)	t_p (psec)	I_B (TW/cm^2)	E_B (MV/cm)	P_B (MW)	ε_B (J/cm^2)
14.0	9.5 ± 0.5	0.88 ± 0.09	15.0 ± 0.7	2.71 ± 0.27	5.01 ± 0.50
	8.5 ± 0.5	0.90 ± 0.09	15.1 ± 0.7	2.77 ± 0.28	8.14 ± 0.82
	6.5 ± 0.5	1.06 ± 0.11	16.4 ± 0.9	3.26 ± 0.33	7.32 ± 0.73
	4.0 ± 0.5	1.8 ± 0.20	21.4 ± 1.2	5.54 ± 0.56	7.66 ± 0.77
7.2	175 ±15	0.88 ± 0.12	15.0 ± 1.2	0.72 ± 0.09	163 ±20
	92 ±15	0.92 ± 0.13	15.3 ± 1.1	0.75 ± 0.10	90 ±12
	47 ± 6	0.96 ± 0.14	15.6 ± 1.0	0.78 ± 0.10	48 ± 7
	9.5 ± 0.5	1.93 ± 0.19	22.1 ± 1.1	1.57 ± 0.16	19.5 ± 2.0
	7.5 ± 0.5	2.05 ± 0.21	22.8 ± 1.2	1.67 ± 0.17	16.3 ± 1.6
	6.5 ± 0.5	2.15 ± 0.22	23.4 ± 1.2	1.75 ± 0.18	14.9 ± 1.5
	5.5 ± 0.5	2.30 ± 0.23	24.2 ± 1.2	1.87 ± 0.19	13.5 ± 1.4
	4.5 ± 0.5	2.89 ± 0.29	27.1 ± 1.4	2.35 ± 0.24	13.8 ± 1.4
	3.5 ± 0.5	3.31 ± 0.33	29.0 ± 1.4	2.69 ± 0.27	12.3 ± 1.2
5.0	9.4 ± 0.5	2.60 ± 0.26	25.7 ± 1.3	1.02 ± 0.10	26.0 ± 0.3
	7.5 ± 0.5	3.26 ± 0.33	28.8 ± 1.4	1.28 ± 0.13	26.0 ± 0.3
	6.5 ± 0.5	3.77 ± 0.38	31.0 ± 1.5	1.45 ± 0.15	26.1 ± 0.3
	5.5 ± 0.5	3.98 ± 0.40	31.3 ± 1.6	1.56 ± 0.16	23.2 ± 0.2
	4.5 ± 0.5	4.49 ± 0.45	33.8 ± 1.6	1.76 ± 0.18	21.5 ± 0.2

Table VII. LID data for sample 82-NC-1 (NaCl) at 1.05 μm.

w (μm)	t_p (psec)	I_B (TW/cm^2)	E_B (MV/cm)	P_B (MW)	ε_B (J/cm^2)
14.0	9.5 ± 0.5	0.25 ± 0.03	8.00 ± 0.44	0.77 ± 0.08	2.55 ± 0.26
	8.5 ± 0.5	0.26 ± 0.03	8.18 ± 0.41	0.81 ± 0.08	2.38 ± 0.24
	7.5 ± 0.5	0.29 ± 0.03	8.50 ± 0.43	0.89 ± 0.09	2.31 ± 0.23
	6.5 ± 0.5	0.37 ± 0.04	9.64 ± 0.57	1.12 ± 0.11	2.55 ± 0.26
	5.5 ± 0.5	0.40 ± 0.04	10.10 ± 0.48	1.23 ± 0.12	2.38 ± 0.24
	4.5 ± 0.5	0.45 ± 0.05	10.70 ± 0.58	1.37 ± 0.14	2.12 ± 0.21
7.2	7.5 ± 0.5	0.66 ± 0.07	12.9 ± 0.73	0.53 ± 0.05	5.22 ± 0.52
	6.5 ± 0.5	0.75 ± 0.08	13.8 ± 0.73	0.61 ± 0.06	5.15 ± 0.52
	5.5 ± 0.5	0.88 ± 0.09	14.9 ± 0.81	0.71 ± 0.07	5.12 ± 0.52
	4.5 ± 0.5	0.97 ± 0.10	15.7 ± 0.80	0.79 ± 0.08	4.65 ± 0.47
	3.6 ± 0.3	1.38 ± 0.14	18.8 ± 0.87	1.12 ± 0.09	5.28 ± 0.53
5.0	7.5 ± 0.5	0.74 ± 0.07	13.7 ± 0.65	0.29 ± 0.03	5.86 ± 0.59
	6.5 ± 0.5	1.00 ± 0.10	15.9 ± 0.83	0.39 ± 0.04	6.91 ± 0.69
	5.5 ± 0.5	1.14 ± 0.11	17.0 ± 0.83	0.45 ± 0.05	6.66 ± 0.67
	4.5 ± 0.5	1.29 ± 0.13	18.1 ± 0.91	0.51 ± 0.05	6.20 ± 0.62

Table VIII. LID data for sample 78-NC-1 (NaCl) at 1.05 μm. The data for the 7.2 μm spot size and t_p = 45 to 167 psec is taken from Ref. 2 and is interpulated from measurements made at spot size of 6.1 and 10.3 μm and a laser wavelength of 1.06 μm.

w (μm)	t_p (psec)	I_B (TW/cm^2)	E_B (MV/cm)	P_B (MW)	ε_B (J/cm^2)
4.0	7.5 ± 0.5	0.26 ± 0.03	8.06± 0.54	0.79 ± 0.08	2.03± 0.20
	6.5 ± 0.5	0.28 ± 0.03	8.44± 0.44	0.86 ± 0.09	1.95± 0.20
	5.5 ± 0.5	0.32 ± 0.03	9.03± 0.44	0.99 ± 0.10	1.87± 0.19
	4.5 ± 0.5	0.38 ± 0.04	9.80± 0.53	1.17 ± 0.12	1.82± 0.18
7.2	167 ± 16	0.083± 0.011	4.6 ± 0.3	0.068± 0.008	14 ± 1.5
	100 ± 10	0.110± 0.008	5.1 ± 0.4	0.090± 0.006	11.7 ± 1.2
	45 ± 3	0.118± 0.018	5.5 ± 0.4	0.096± 0.010	5.56± 0.60
	6.5 ± 0.5	0.58 ± 0.06	12.2 ± 0.6	0.43 ± 0.04	4.00± 0.40
	5.5 ± 0.5	0.66 ± 0.07	12.9 ± 0.73	0.53 ± 0.05	3.83± 0.38
	4.5 ± 0.5	0.80 ± 0.08	14.3 ± 0.63	0.65 ± 0.07	3.83± 0.38
	3.5 ± 0.5	0.95 ± 0.10	15.5 ± 0.64	0.77 ± 0.08	3.56± 0.36
5.0	7.5 ± 0.5	0.92 ± 0.09	15.3 ± 0.73	0.36 ± 0.04	7.30± 0.73
	6.5 ± 0.5	0.94 ± 0.09	15.5 ± 0.69	0.37 ± 0.04	6.53± 0.65
	5.5 ± 0.5	1.13 ± 0.11	17.0 ± 0.76	0.44 ± 0.04	6.62± 0.66
	4.5 ± 0.5	1.20 ± 0.12	17.5 ± 0.83	0.47 ± 0.05	5.78± 0.58
	3.4 ± 0.1	1.60 ± 0.16	20.2 ± 0.94	0.63 ± 0.06	5.78± 0.58

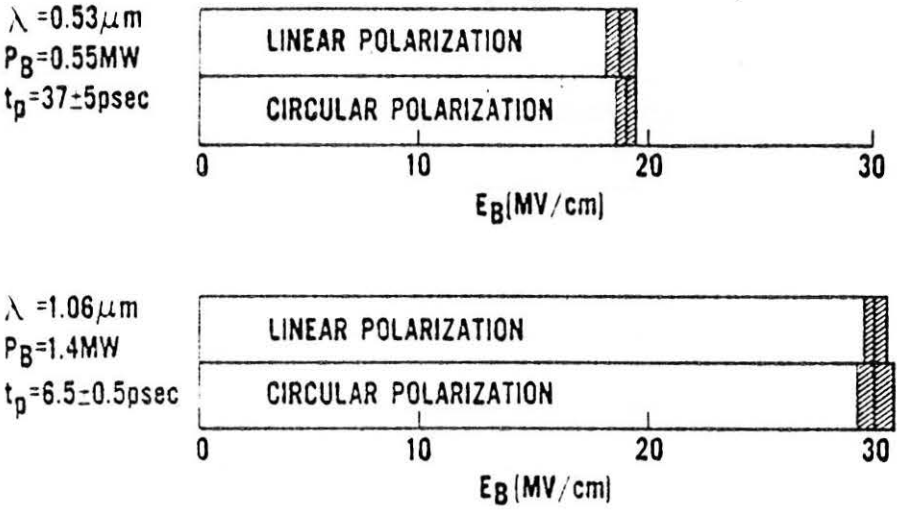

Figure 1. Polarization dependence of E_B for SiO_2. The horizontal axis is E_B, the r.m.s. breakdown field corresponding to the peak on-axis irradiance at damage. P_B is the breakdown threshold power. Note the lack of polarization dependence for both wavelengths. The cross-hatched portions shown above are the relative uncertainties of the thresholds using the procedures given in Ref. 16.

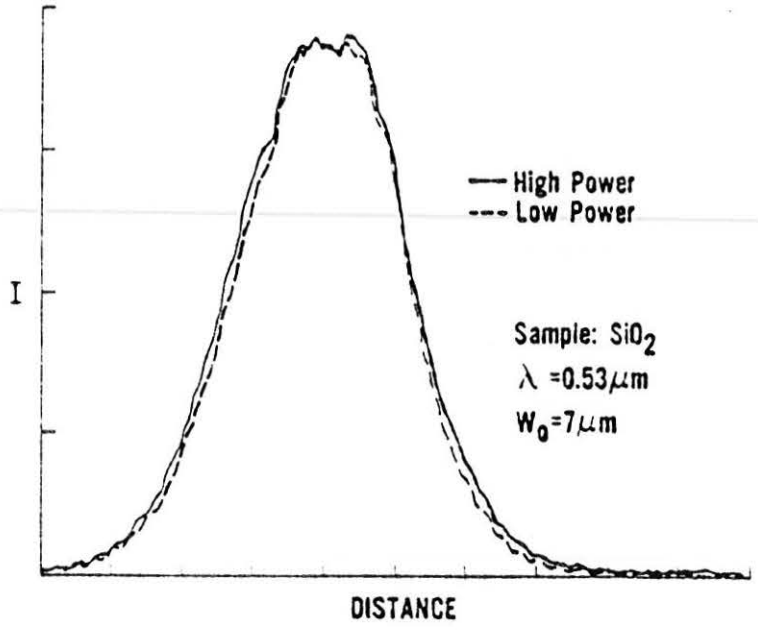

Figure 2. Beam distortion measurements. This is a plot of the far field beam profile of the 0.53 μm beam after propagation through the SiO_2 sample. The quantity w_0 = 7 μm is the focal spot radius inside the sample calculated using linear Gaussian optics. The curve labeled high power was taken with the input power at the damage threshold level and the one labeled low power was for input power approximately equal to one-tenth the damage threshold power.

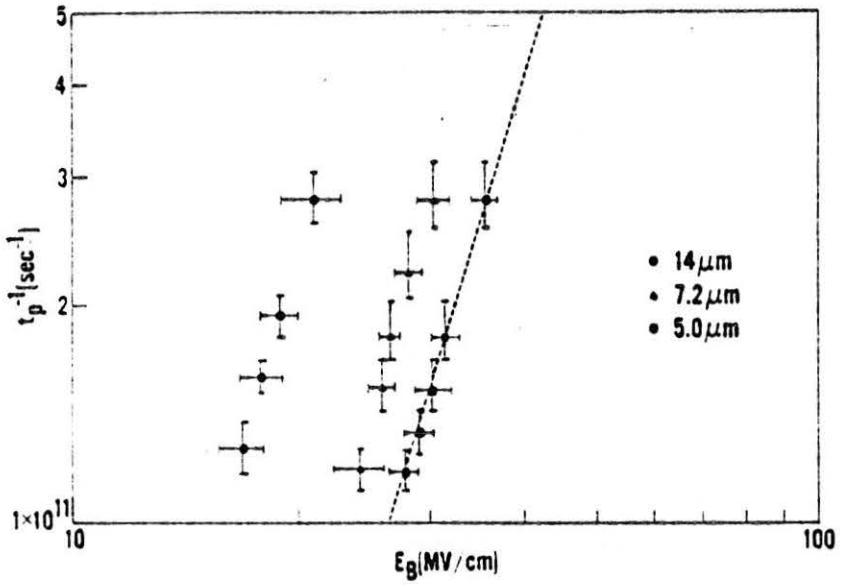

Figure 3. Pulsewidth dependence of E_B for SiO_2 at 1.05 um. The three sets of points correspond to different focal spot radii and the relatively large displacement of the three sets of points is indicative of a large spot size dependence in the damage threshold. The slope of the least square fit for each set of points is approximately 0.3 for this pulsewidth range (t_p < 10 psec).

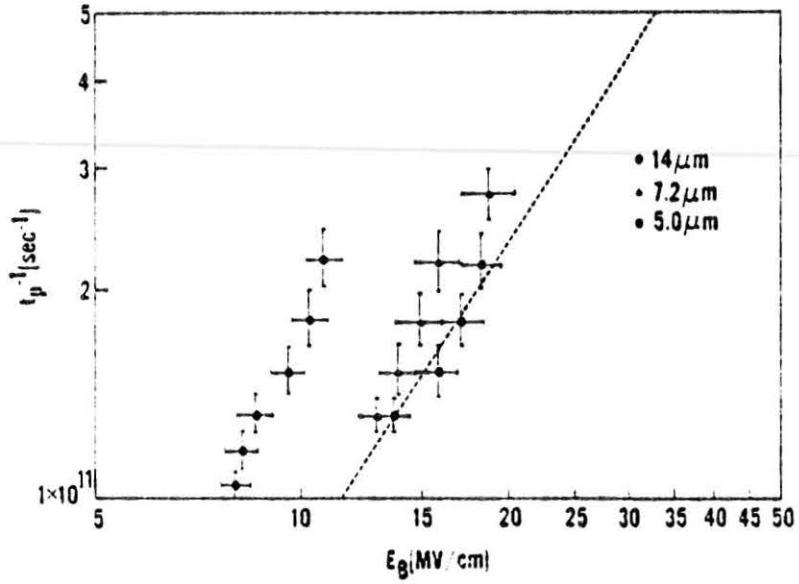

Figure 4. Pulsewidth dependence of E_B in NaCl at 1.05 um. The slope of the least square linear fit to each of the three sets of points is approximately 0.5. This indicates an inverse square root of pulsewidth dependence of E_B for this pulsewidth range (t_p < 10 psec).

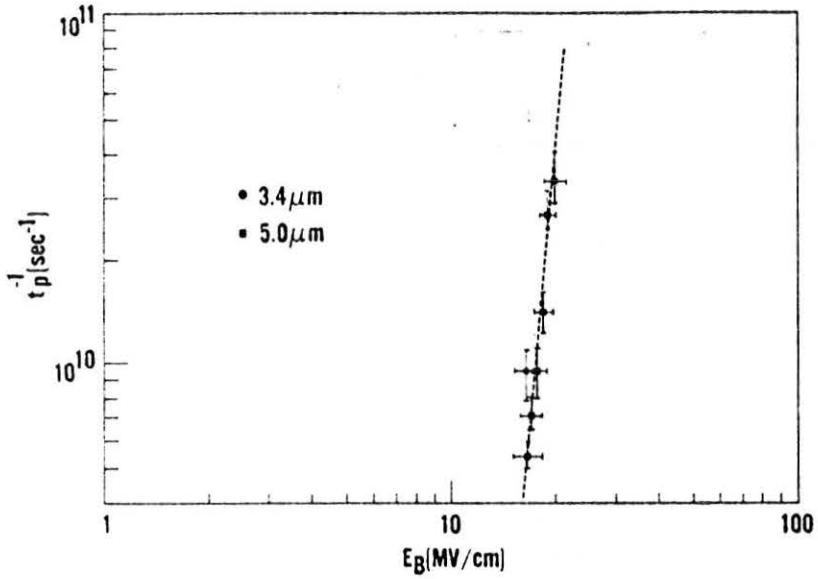

Figure 5. Pulsewidth dependence of E_B in SiO_2 at 0.53 μm. Note E_B is nearly independent of t_p in this pulsewidth range (20 to 300 psec) and that there is little spot size dependence in E_B for the two spot sizes shown (3.4 and 5.0 μm).

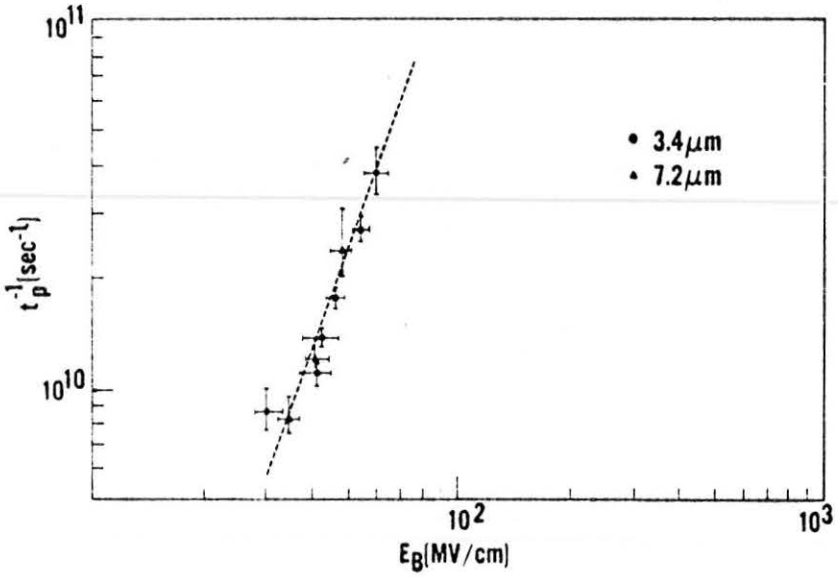

Figure 6. Pulsewidth dependence of E_B in NaCl at 0.53 μm. Note that there is little spot size dependence in E_B for the two spot sizes shown (3.4 and 7.2 μm). The least squares linear fit of these data give a slope of 0.3, or nearly an inverse fourth root dependence of E_B on t_p for pulsewidths in this range (20 to 200 psec).

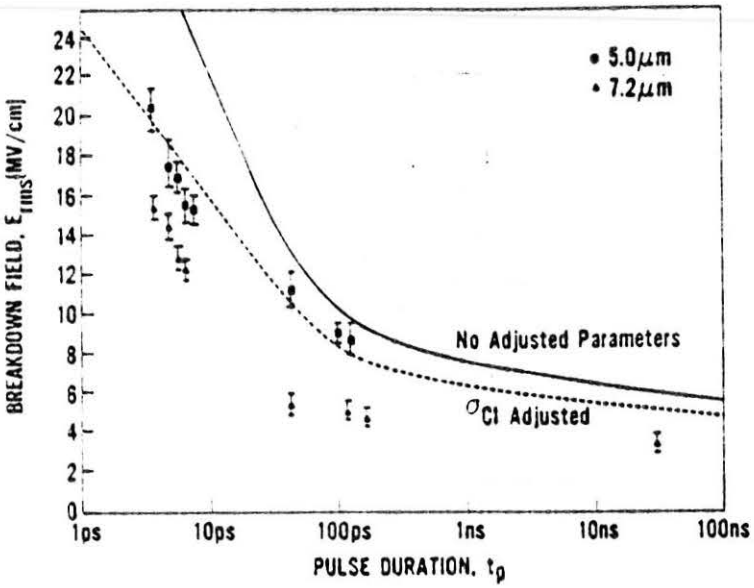

Figure 7. The RMS breakdown field data for NaCl (78-NC-6) at 1.06 μm are plotted as a function of pulse duration, t_p. The solid line and dotted line were obtained from the theory developed by Sparks et al. [28] for NaCl at room temperature. The dotted line uses a different value for the absorption cross section for Cl ions in the theory than the solid line.

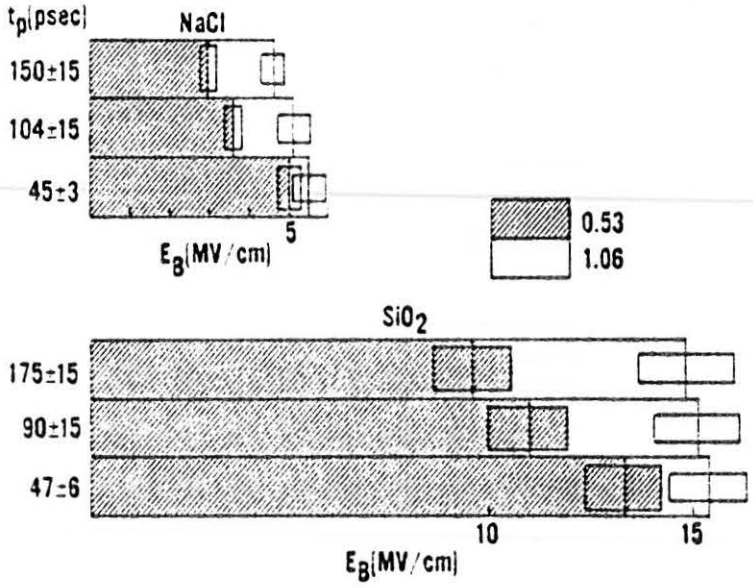

Figure 8. Wavelength dependence of the breakdown field E_B for NaCl and SiO_2 for a variety of laser pulsewidths. All the above data was taken on the same sample of NaCl and the same sample of SiO_2. The 1.06 μm thresholds are taken from Ref. 2 and are interpolated from measurements made at spot size 6.1 and 10.3 μm.